Uptake of Gold Nanoparticles in Healthy and Tumor Cells Visualized by Nonlinear Optical Microscopy

ARTICLE *in* THE JOURNAL OF PHYSICAL CHEMISTRY B · APRIL 2011

Impact Factor: 3.3 · DOI: 10.1021/jp2009012 · Source: PubMed

7 AUTHORS, INCLUDING:

Gianluca Rago
Max Planck Institute for Polymer Research
17 PUBLICATIONS **224** CITATIONS
SEE PROFILE

Mischa Bonn
Max Planck Institute for Polymer Research
347 PUBLICATIONS **7,569** CITATIONS
SEE PROFILE

Annika Enejder
Chalmers University of Technology
55 PUBLICATIONS **1,363** CITATIONS
SEE PROFILE

THE JOURNAL OF PHYSICAL CHEMISTRY B

ARTICLE

pubs.acs.org/JPCB

Uptake of Gold Nanoparticles in Healthy and Tumor Cells Visualized by Nonlinear Optical Microscopy

Gianluca Rago,[†] Brigitte Bauer,[‡] Fredrik Svedberg,[§] Linda Gunnarsson,[¶] Marica B. Ericson,[‡] Mischa Bonn,[†] and Annika Enejder*[,§]

[†]FOM Institute for Atomic and Molecular Physics AMOLF, 1098XG Amsterdam, The Netherlands

[‡]Biomedical Photonics, Department of Physics, University of Gothenburg, 412 96 Göteborg, Sweden

[§]Molecular Microscopy, Department of Chemical and Biological Engineering, Chalmers University of Technology, 412 96 Göteborg, Sweden

[¶]Bionanophotonics, Department of Applied Physics, Chalmers University of Technology, 412 96 Göteborg, Sweden

Supporting Information

ABSTRACT: Understanding the mechanism underlying the interactions between inorganic nanostructures and biological systems is crucial for several rapidly growing fields that rely on nano-bio interactions. In particular, the further development of cell-targeted drug delivery using metallic nanoparticles (NP) requires new tools for understanding the mechanisms triggered by the contact of NPs with membranes in different cells at the subcellular level. Here we present a novel concept of multimodal microscopy, enabling three-dimensional imaging of the distribution of gold NPs in living, unlabeled cells. Our approach combines multiphoton induced luminescence (MIL) with coherent anti-Stokes Raman scattering (CARS) microscopy. Comparison with transmission electron microscopy (TEM) reveals in vivo sensitivity down to the single nanostructure. By monitoring the incorporation of NPs in human healthy epidermal keratinocytes and squamous carcinoma cells (SCC), we address the feasibility of noninvasive delivery of NPs for therapeutic purposes. While neutralizing PEG coating was confirmed to prevent NP integration in SCCs, an unexpectedly efficient integration of NPs into keratinocytes was observed. These results, independently validated using TEM, demonstrate the need for advanced surface modification protocols to obtain tumor selectivity for NP delivery. The CARS/MIL microscopy platform presented here is thus a promising tool for noninvasive study of the interaction between NPs and cell.

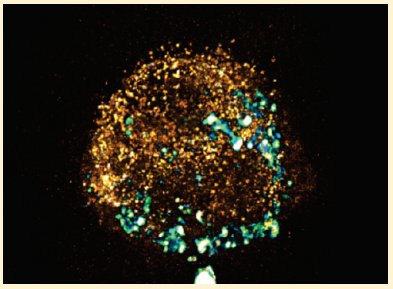

INTRODUCTION

Gold nanoparticles (AuNPs) have recently emerged as a compelling alternative for cell-targeted therapeutic delivery[1] and diagnosis.[2] In contrast to polymer- and liposome-based vehicles, AuNPs can inherently be tracked using microscopy techniques without the involvement of bulky reporter molecules. Contrary to fluorophores, they emit a stable and intense optical photoluminescence signal without photobleaching or blinking effects. Moreover, the photoluminescence can be significantly enhanced through the coupling to localized surface plasmon modes of the AuNPs.[3] In addition, AuNPs are biologically nontoxic,[4] as opposed to, e.g., carbon nanotubes[5] and quantum dots,[6] which generally contain heavy metals. The near atomic-scale specificity with which AuNPs can be manufactured enables fine-tuning of their size and shape[7] for efficient integration into cells, further supported by tailored surface properties by attaching antibodies, peptides, oligonucleotides, oligosaccharides, and lipids.[8−16] By further functionalizing these constructs with enzymes,[17] drugs, and gene-regulating biomolecules (for recent reviews, see refs 1 and 18), AuNPs can serve as vehicles for cell-specific therapeutics, with the advantages of highly localized and controlled release of the active component along with reduced systemic dosing. Within this context, special attention has been given to selective targeting of tumor cells[19−21] and functionalization of AuNPs with anticancer drugs[22−28] for cancer treatment.

These application-oriented studies imply that functionalized AuNPs will enable important contributions to modern health care. In order to exploit the full potential of AuNPs, extensive efforts are now being invested to establish a fundamental understanding of the general mechanisms behind their transmembrane transport, cytoplasmic trafficking, and intracellular processing. Present knowledge relies primarily on observations made by transmission electron microscopy (TEM), frequently supported by inductively coupled plasma atomic emission spectroscopy (ICP-AES).[7] While the latter technique provides the average AuNP population uptake at a given time without information on the intracellular localization, TEM has the ability to resolve both AuNPs and cellular features in the nanometer range. Although TEM therefore has contributed significantly to our understanding of AuNP−cell interaction, some significant limitations may

Received: January 27, 2011
Revised: March 14, 2011

dx.doi.org/10.1021/jp2009012 | J. Phys. Chem. B XXXX, XXX, 000–000

be noted: the sample preparation procedure involving cell fixation, metal deposition, resin embedding, and slicing of the cell is time consuming and highly invasive, and has been previously associated with potential artifacts.[29] In addition, TEM measurements are performed on thin subsections of the cell (typically 80 nm in width), granting the technique high axial resolution with the downside that a study of the entire volume of a single cell requires the measurement of a large number of subsections.

An alternative strategy is to use optical microscopy. By coupling a fluorescent reporter molecule to the NPs, their uptake in living cells has been followed by fluorescence[30] and Raman[31] microscopy. However, some drawbacks of this approach may be noted: first, considering the decisive role of NP surface chemistry for the interaction process, it is not completely evident that the marker is not affecting the uptake process. Second, the risk exists that the reporter molecules decouple from the NPs throughout the integration process and that an erroneous picture of the incorporation is obtained. In addition, long-term studies are not possible since fluorophores bleach, get quenched, and induce phototoxic reactions.

In the light of these considerations, label-free imaging utilizing the intrinsic optical properties of AuNPs appears as an attractive alternative. For instance, their strong light diffraction renders AuNPs visible in dark-field microscopy,[32,33] though merely as a two-dimensional projection and unrelated to the cell morphology since no contrast is given by the low-diffractive cellular features. Thus, no true nano−bio correlation can be achieved here. AuNPs are also intrinsically photoluminescent upon laser irradiation,[34] though in general too weak for live cell imaging. By instead exciting the AuNPs through a multiphoton process using NIR light, the photoluminescence efficiency is significantly enhanced for particles in a broad dimensional range due to the coupling to the localized surface plasmon modes.[35,36] Multiphoton induced luminescence (MIL) has indeed successfully been exploited for the visualization of gold nanorods in A431 skin cancer cells,[37] generating a signal >4000 times brighter than that from intrinsic fluorophores, and of gold nanoparticles in endothelial cells.[38] However, again only the AuNPs were visualized, without being related to the biological context and limited to subsections of the cells. The label-free visualization of live cells has recently been demonstrated using coherent anti-Stokes Raman scattering (CARS) microscopy[39] and makes use of similar light sources as those required for MIL.

By combining MIL and CARS, we are able to visualize the full three-dimensional distribution of AuNPs simultaneously within their cellular environment without any labeling. The CARS process is based on the interaction of two pulsed laser beams with the sample. When their frequency difference matches a vibrational resonance of a specific molecular bond, an enhanced blue-shifted signal is emitted from the high-intensity region of the focal spot only. This provides axial sectioning capabilities and a lateral resolution corresponding to ∼300 nm. By coupling the beams into a scanning microscope, label-free, three-dimensional imaging of the target molecule, here lipids,[40] in living samples is achieved at submicrometer resolution and video rate.[41−43] With the use of NIR laser light, the multiphoton luminescence process is simultaneously induced in the AuNPs, forming corresponding three-dimensional images of their distribution which can be colocalized with the lipid-rich cell membranes and organelles visualized in the CARS volume images. The combination of MIL and CARS is in principle a suitable mean for the visualization in cells of other plasmonic particles that exhibit large luminescence response, e.g., silver nanoparticles.[44]

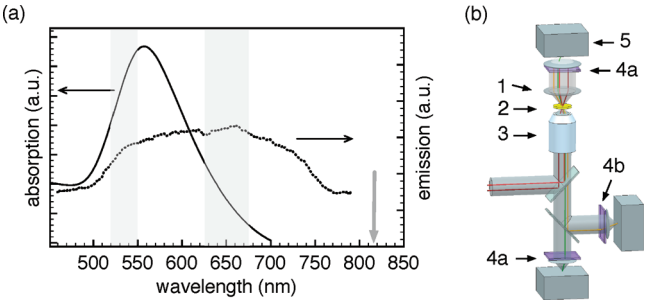

Figure 1. (a) Absorption (filled line) and emission (dashed) spectra of a water solution of PEG-coated, 60 nm sized AuNPs. While the maximum can be found at 560 nm, the light absorption is still significant in the multiphoton excitation region. The multiphoton-induced photoluminescence emitted following excitation at 817 nm (gray arrow) shows a broad spectral character. The gray areas indicate the spectral regions used for MIL detection. (b) Schematic illustration of the CARS/MIL microscope. The excitation beams (817 and 1064 nm, respectively) from the laser system are coupled into the microscope by a mirror scanner. The CARS-signal is detected by the PMT (band-pass filter 625−675 nm) in transmission mode and the two MIL signals by the dual-channel detection arrangement (520−550 nm and 625−675 nm, respectively) in reflection mode. (1) Condenser; (2) sample; (3) objective; (4a) band-pass filter 625−675 nm; (4b) band-pass filter 520−550 nm; (5) PMT.

As a first important application, we study the integration and distribution of poly(ethylene glycol) (PEG)-coated AuNPs in human squamous carcinoma cells (SCC) (A431 skin cancer cell line) and healthy keratinocytes in order to address the feasibility of transdermal delivery of AuNP therapeutic and diagnostic agents in particular for cancer treatment, as only limited studies entail a comparison between tumor cells and normal cells. The observations reported here were confirmed with high-resolution transmission electron microscopy (TEM).

MATERIALS AND METHODS

Preparation of AuNPs. Sixty nanometer colloidal gold particles (BB International, Cardiff, UK) were coated with a monolayer of thiol-conjugated PEG, SH-PEG (MW 5000 g mol^{-1}, Sigma, St. Louis, MO), known to reduce nonspecific cell integration and to prevent AuNP aggregation. The commercial colloidal solution was centrifuged and the supernatant was removed. An aliquot of 1 mL of 0.15 μg/mL SH-PEG dissolved in Milli-Q water was added to the particle pellet and left to incubate overnight for monolayer formation. After incubation, the colloidal solution was centrifuged and the supernatant was removed and replaced with ∼1 mL of fresh Milli-Q water. The extinction coefficient of the PEG-coated AuNPs was measured in a Cary 5000 UV−vis spectrophotometer. The absorption maximum was centered at approximately 555 nm, with a full width at half-maximum (fwhm) of ∼100 nm (Figure 1a). The corresponding emission spectra, excited by the OPO output at 817 nm, were measured by a fiber-based spectrometer (AvaSpec 2048, Avantes, Eerbeek, The Netherlands) coupled to the microscope, resulting in a broad photoluminescence continuum ranging between 500 and 760 nm (Figure 1a), spectrally limited by collection optics and filters.

Cells. Normal human epidermal keratinocytes (HEKs, Cascade Biologics, Portland, OR) were maintained in phenol-red-free

dx.doi.org/10.1021/jp2009012 |J. Phys. Chem. B XXXX, XXX, 000–000

EpiLife keratinocyte medium (Cascade Biologics, Portland, OR) supplemented with 60 μM $CaCl_2$, gentamicin/amphotericin and 1% (v/v) human keratinocyte growth supplement (HKGS; Cascade Biologics) at 37 °C and in a 5% CO_2 incubator. Final concentrations of the components in the supplemented medium were as follows: bovine pituitary extract, 0.2% v/v; bovine insulin, 5 mg/mL; hydrocortisone, 0.18 mg/mL; bovine transferrin, 5 mg/mL; human epidermal growth factor, 0.2 ng/mL; gentamicin, 10 μg/mL; and amphotericin B, 0.25 μg/mL. The keratinocytes were used for experiments in the fifth or sixth passage. Human squamous carcinoma cells (A431, HPA cultures, Salisbury, UK) were maintained in phenol-red-free Eagles's Minimum Essential Medium (EMEM, Invitrogen, Pailsey, UK), supplemented with 10% fetal bovine serum, 2 mM glutamine EMEM, and 1% nonessential amino acids (NEAA) at 37 °C and in a 5% CO_2 incubator. Both cell lines were seeded on 35 mm diameter glass bottom dishes (P35G-1.5-14-C; MatTek, Ashland, MA) at a density of 1×10^3 cells/cm^2. After 3 days, cells were incubated in growth medium with 10% (v/v) solution containing PEG-coated 60 nm gold nanoparticles (2.6×10^{10} particles/mL, corresponding to 43.1 pM) for 2, 6, and 10 h, respectively. For the CARS/MIL microscopy, the incubation medium was removed, after which the cell layer was washed two times with 1 mL of HEPES imaging buffer (140 mM NaCl, 20 mM HEPES, 5 mM KCl, 1 mM $MgCl_2$, 0.06 mM $CaCl_2$, 10 mM D-Glucose), and then immersed in 2 mL of imaging buffer. For TEM, the incubation medium was instead replaced overnight with a mixture of 2% paraformaldehyde, 2.5% glutaraldehyde, and 0.02% sodium azide in 0.05 M sodium cacodylate buffer, pH 7.2. Postfixation was performed for 2 h at 4 °C with 1% osmium tetroxide and 1% potassium ferrocyanate in 0.1 M cacodylate. After rinsing, the specimens were treated for 1 h with 0.5% uranyl acetate in water. Dehydration was performed in a graded series of ethanol followed by acetone and epoxy resin (Agar 100; Agar Scientific, Stansted, UK) infiltration. The plastic was cured by heat. After removal of the embedded cultures from the culture dishes, ultrathin sectioning was performed with a Leica EM UC7 ultramicrotome (Leica Microsystems, Vienna, Austria), parallel with and perpendicular to the culture surface. Diamond knives were used at a section thickness setting of 60 nm.

CARS and MIL Microscopy. The microscopy setup consists of a picosecond pulsed laser system generating two synchronized beams collinearly aligned into an inverted microscope (Eclipse TE-2000, Nikon, Tokyo, Japan) via a beam scanning unit (C1, Nikon). A fraction of the fundamental output of a Nd:Van laser (Picotrain, HighQ Lasers GmbH, Hohenems, Austria) at 1064 nm is directly coupled into the microscope serving as the Stokes beam in the CARS process, while its frequency-doubled output (532 nm) is used to synchronously pump an optical parametric oscillator (Emerald OPO, APE GmbH, Berlin, Germany). The tunable output is provided by the OPO, set to 817 nm in this work to form a beating excitation field with the Stokes beam at the frequency 2845 cm^{-1} corresponding to the resonant vibration of the CH_2 group in the acyl chain of lipids, so that CARS images predominantly organelles with high lipid content. The laser beams were focused on the sample by an oil immersion objective (Plan Fluor 40×, NA 1.30, Nikon), resulting in a power of 10 mW for each of the beams at the sample position. The CARS signal was collected by an aspherical lens (NA 0.68) in the forward direction and detected by a single-photon counting photomultiplier tube (PMC-100, Hamamatsu) connected to a time-correlated single-photon-counting unit (SPCM-830, Becker and Hickl). Band-pass filters in front of the detector suppressed the radiation at the laser wavelengths and preferentially transmitted the CARS signal generated at 663 nm. A detailed outline of the setup has been given by Enejder et al.[40] In the same experimental configuration, i.e., on the same sample, in the same region within the sample, the MIL signal from the AuNPs was obtained by single-beam excitation using the OPO output (817 nm). In these experiments, the 1064 nm beam was blocked in order to exclude any contributions from CARS-generating objects. Following multiphoton absorption, the AuNPs emitted a photoluminescence detected in epi geometry. Its broadband character in the wavelength region characteristic for 60 nm sized AuNPs was ascertained by a dual-channel detection arrangement, consisting of two sets of band-pass filters (535/25 nm and 650/50 nm, Chroma Technologies, USA), each in front of a single-photon-counting PMT connected to the SPCM unit. By time-gating, the impact of autofluorescence from the biological environment on the instantaneous photoluminescence could be minimized. Three-dimensional imaging was achieved by scanning a sequence of horizontal planes at different vertical positions by translating the objective with a motorized stage. Rapidly switching between CARS and MIL microscopy mode was achieved by simply selecting appropriate combinations of excitation beams as illustrated in Figure 1b, assuring that the CARS and MIL images were collected from the same region. In a future development, this can be achieved at single-pulse level by an acousto-optical pulse-selection unit, enabling simultaneously recorded CARS and MIL images. Samples were first imaged in brightfield white-light microscopy, and the areas of interest, typically covering 60×60 μm^2 (256×256 pixels), were then imaged at different vertical positions with 1 μm spacing by CARS and MIL microscopy. The total acquisition time for each layer was 20 s for each of the techniques.

TEM. The sections of the cells were collected on copper grids with an area of 3 mm^2 and contrasted with uranyl acetate and lead citrate before examination in a Zeiss 912AB electron microscope (Carl Zeiss SMT AG, Oberkochen, Germany) equipped with a LaB_6 electron source operated at at 120 kV. Images were collected using a MegaView III CCD camera (Olympus SIS, Münster, Germany). For each experiment (keratinocytes/SCC; 2, 6, 10 h incubation), three copper grids containing eight slices each (24 slices per experiment) were investigated to find cells containing nanoparticles. Areas with NPs were zoomed in and investigated in more detail. On average, images of 2−3 cells containing NPs were collected for each experiment.

RESULTS

To first establish the capability of combining CARS and MIL, a series of images of A431 squamous carcinoma cells (SCCs) incubated with AuNPs for 6 h was collected. Figure 2a shows the forward-emitted CARS signal collected at the CH-stretch vibration at 2845 cm^{-1} obtained from a cluster of SCCs. As shown by the figure, CARS microscopy visualizes lipid-rich biological structures such as cell membranes and lipid-rich intracellular components, which here appear as high-intensity regions in the cell cluster. The CARS images thereby provide the biological frame of reference for the nano−bio interaction, so that the relative location of NPs within cells can be determined with the use of MIL. The corresponding photoluminescence images,

dx.doi.org/10.1021/jp2009012 |J. Phys. Chem. B XXXX, XXX, 000–000

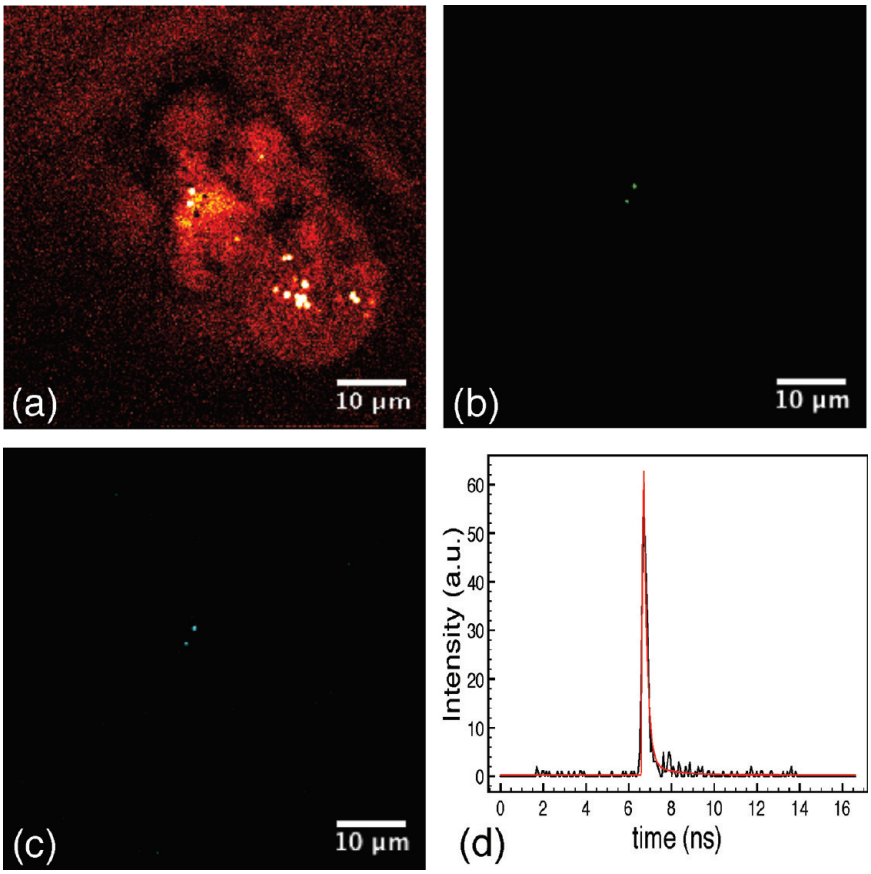

Figure 2. A set of CARS and MIL microscopy images of squamous carcinoma cells incubated with PEG-coated AuNPs for 6 h. Images are a subset of three stacks, each covering a total volume of 60 × 60 × 30 μm (256 × 256 × 30 pixels) forming tomographic images of the cells and the distribution of the AuNPs. (a) Forward-emitted CARS signal collected at the CH vibration 2845 cm^{-1}, visualizing organelles with high lipid content. (b,c) Epi-detected MIL signals collected in spectral regions around (b) 535 nm and (c) 650 nm at corresponding vertical position. (d) Time decay of the MIL signal collected at the location of one of the bright spots in the 535 nm MIL image, proving the short lifetime characteristic of photoluminescence and the limited contribution from fluorescence.

shown in Figure 2b,c, were recorded from the same sample by the dual-detector arrangement at 535/25 and 650/50 nm. Two features with lateral dimensions smaller than 1 μm located at the same positions in the sample can be observed in both the 535 and 650 nm images. This confirms that the emission from the features are of broad spectral character in a wavelength region typical for the photoluminescence of 60 nm sized AuNPs supported by the spectrum in Figure 1b. Time-resolved measurements further confirmed the photoluminescent origin of the emission from the two features in the MIL images. Fitting the time decay shown in Figure 2d with a single-exponential function results in an ultrashort decay time <200 ps, characteristic for photoluminescence of gold nanostructures.[45,46] The location of the AuNPs within the cells could be determined with high *accuracy* by overlaying the two images. Isolated AuNPs were represented as spots of average size of ~300 nm in the $x-y$ plane and ~1 μm in depth, which represents the point spread function of MIL. The resolution of CARS microscopy is reported to be comparable by others.[47]

In order to investigate the *sensitivity* with which AuNPs can be visualized, a comparison was made with TEM images of the corresponding cellular system; SCCs incubated for 6 h. A 60 nm thick vertical cut of the SCCs reveal a AuNP embedded in multivesicular compartments of the average size ~300 nm, located in the vicinity of the nucleus, as exemplified in Figure 3a. A high-resolution TEM image, as exemplified in Figure 3b, further reveal the multivesicular nature of the compartment, suggesting that the AuNPs are mainly in the later stage of the endosomal degradation pathway[48] after 6 h of incubation. No formation of AuNP clusters was observed in SCC slices, confirming that the features visualized in the MIL images indeed represent individual AuNPs.

The kinetics of the AuNP integration process were investigated by collecting CARS/MIL and TEM images after the incubation at 2, 6, and 10 h, respectively. The full series of events for the SCCs is depicted in the overlay CARS/MIL images in Figure 4, including corresponding orthogonal side views reconstructed from the stacks (60 × 60 × 20 μm^3 for Figure 4a,b, and 60 × 60 × 30 μm^3 for Figure 4c). The images confirm the low uptake of AuNPs indicated in Figure 3, both at shorter (2 h) and longer (10 h) incubation times. Independent of the incubation time, two populations can be identified; the AuNPs are either localized at the cell membrane or in endosomes in the perinucleic region of the cell. In Figure 4a (2 h), a single AuNP can be observed in the horizontal plane ($x-y$ projection) at the top of the image as well as in the side $y-z$ projection localized in the vicinity of the outer cellular membrane, whereas the side $x-z$ projection also shows a AuNP in the perinucleic region. After 2 h of incubation, three out of six of the SCCs that were investigated

dx.doi.org/10.1021/jp2009012 |*J. Phys. Chem. B* XXXX, XXX, 000–000

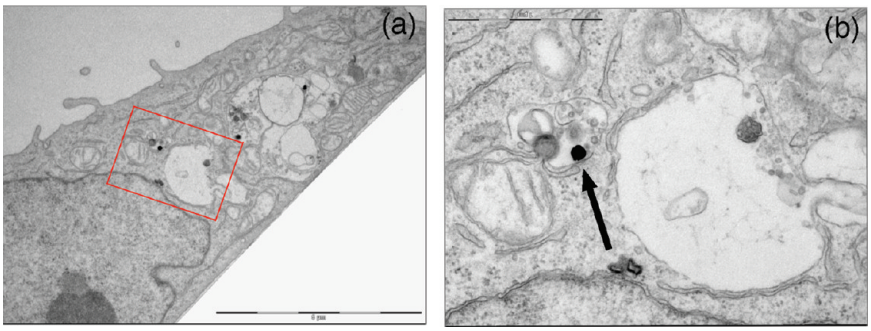

Figure 3. (a) TEM image of a vertical cut of a squamous carcinoma cell incubated with PEG-coated AuNPs for 6 h. Scale bar 5 μm. (b) Enlargement of a perinucleic area containing a single AuNP in a multivesicular endosome. Scale bar 1 μm.

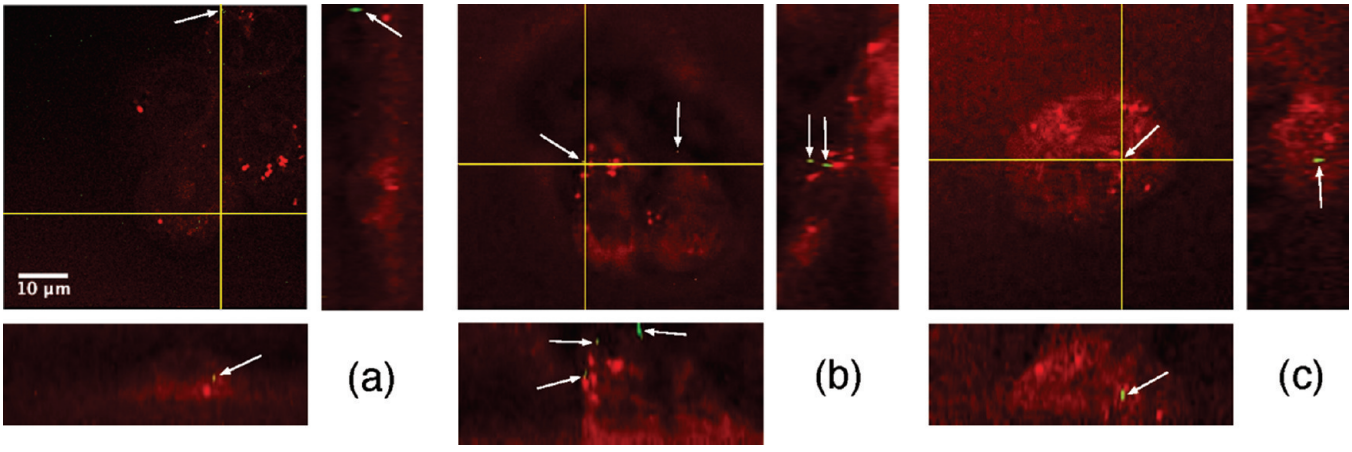

Figure 4. Overlay CARS (red) and MIL (green) images of SCCs with corresponding orthogonal side views collected after (a) 2 h, (b) 6 h, and (c) 10 h incubation with PEG-coated AuNPs, respectively. The lines in the front views indicate the position of the orthogonal projections. Two isolated MIL signals attributed to luminescence from AuNPs can be distinguished in the cells in (b) after 2 h of incubation, four in the cells in (c), and one intracellular spot in (c) after 10 h of incubation, indicated by arrows.

contained no AuNPs, and the other three contained either one or two AuNPs. Two to three AuNPs are visible in each of the projections in Figure 4b (6 h), again localized either at the cell membrane or in the cytoplasm, preferentially close to the nucleus. After 6 h of incubation, two or three NP signatures were observed in four out of six cells. Finally, in Figure 4c (10 h) one AuNP is visible in each of the projections, localized in the proximity to the nucleus. Here, between three and seven intracellular AuNPs could be observed in the SCCs investigated. From the entire set of CARS/MIL images of SCCs, it is evident that the number of isolated MIL emitters representing AuNPs increases slightly with the incubation time, but remains in a range between 1 and 7. This figure includes the particles that were visible close to the outer cell membrane, thus probably still membrane bound rather than internalized. The limited unspecific uptake of PEG-coated AuNPs was confirmed by TEM for all incubation times; careful inspection of all 60 nm thin slices (72 slices in total) revealed NPs in a single cell, here enclosed in multivesicular perinucleic 300 nm sized endosomes. No particles were observed in the nucleus, irrespective of microscopy technique used.

The interaction of the PEG-coated AuNPs with the human epidermal keratinocytes was found to be of a significantly different character, as illustrated by the CARS/MIL projections (horizontal planes and corresponding orthogonal side views) in Figure 5. The corresponding TEM images confirm this scenario. As opposed to SCCs, NPs were readily located in the keratinocytes and observed in a majority of the 72 slices. Given the generally low probability to find NPs in such thin slices (60 nm), this observation indicates a significant uptake capability of the keratinocytes. In order to ascertain that the difference is not due to differences in PEG-coating, experiments were performed in duplicates.

Already following 2 h incubation, a few AuNPs (maximum six features per cell in a total of five cells) were observed in the CARS/MIL images of the keratinocytes (Figure 5a), primarily located in the vicinity of the cell membrane. The corresponding TEM images confirm this as exemplified in Figure 5d; a single AuNP (see arrow) can be here noted close to the cellular membrane. After an incubation time of 6 h (Figure 5b), several tens of luminescent features with submicrometer lateral dimensions were found to be present inside the cell for all six cells investigated. The AuNPs were evenly distributed throughout the cytoplasmatic area, though without entering the nucleus. TEM images of corresponding cells (Figure 5e) confirm the presence of multiple isolated AuNPs internalized in endosomes of sizes varying between 300 and 800 nm distributed in the cytoplasm. CARS/MIL images of the keratinocytes incubated for 10 h (Figure 5c) show a high density of AuNPs, especially in the perinucleic region. Even micrometer-sized clusters can be observed in the cytoplasm, characterized by an average count per

dx.doi.org/10.1021/jp2009012 |J. Phys. Chem. B XXXX, XXX, 000–000

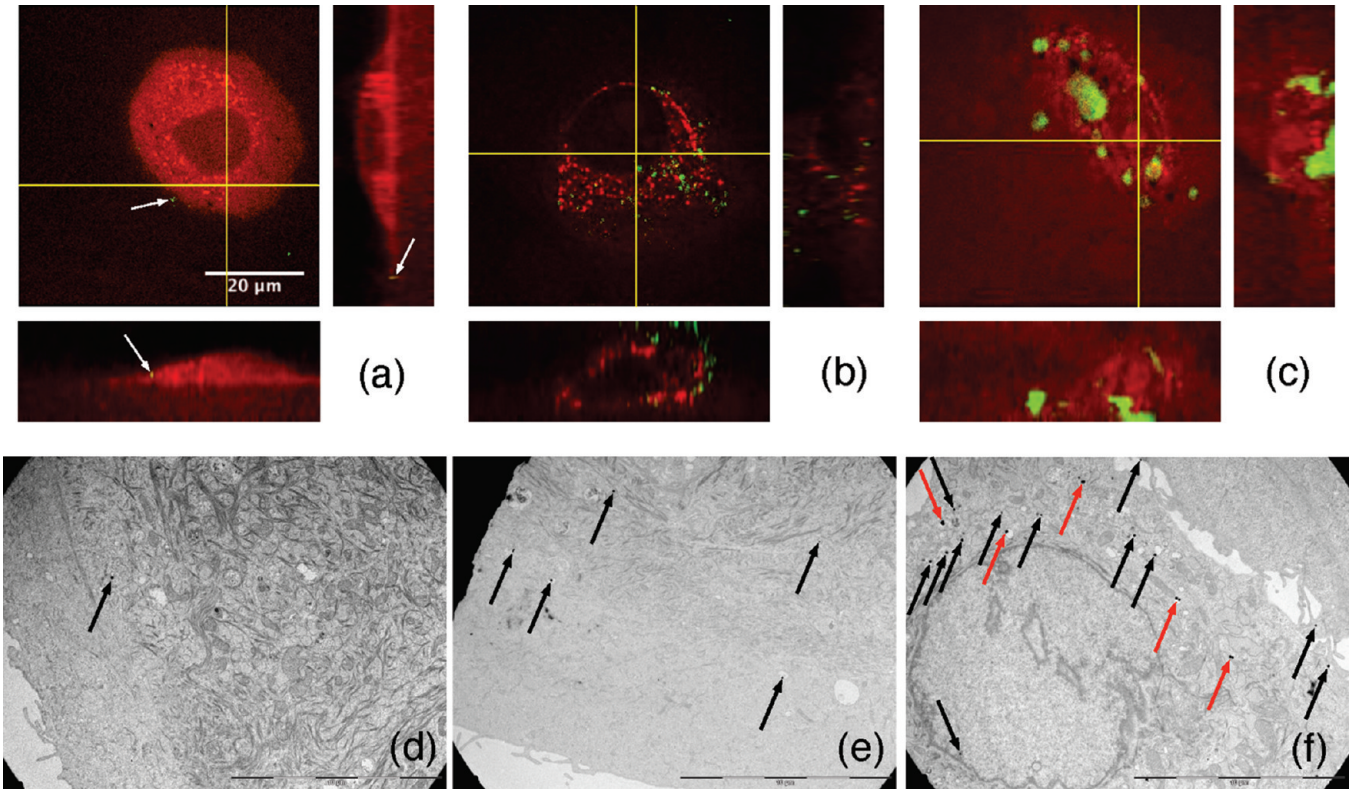

Figure 5. Overlay CARS (red) and MIL (green) images of human epithelial keratinocytes with corresponding orthogonal side views collected after (a) 2 h, (b) 6 h, and (c) 10 h incubation with PEG-coated AuNPs, respectively. Three isolated MIL signals attributed to luminescence from AuNPs can be distinguished at the cell membrane in (a) after 2 h of incubation (white arrows), multiple intracellular AuNPs in (b) after 6 h, and clusters of AuNPs in (c) after 10 h (discussed in the text). (d–f) TEM images of cells incubated corresponding times (scale bar 5 μm). Black arrows indicate individual AuNPs. In (f), clusters of AuNPs can also be observed (red arrows).

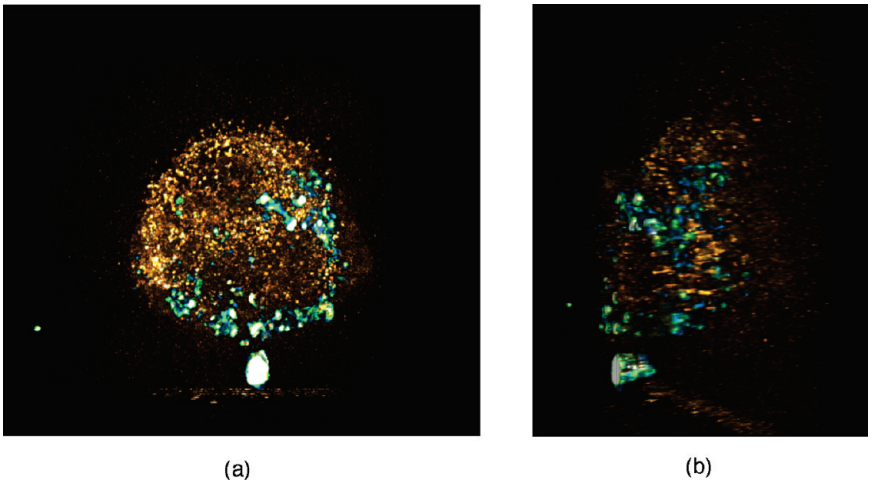

Figure 6. Three-dimensional CARS/MIL overlay images of HEK incubated with PEG-coated AuNPs for 6 h. The images cover a volume of 60 × 60 × 20 μm.

pixel of approximately 3 times that recorded from the spots identified as single AuNPs. In this case, MIL features have dimensions much larger than the diffraction limit, preventing an average quantification. The same behavior was found in the three cells investigated. The corresponding TEM images partly confirm this picture (Figure 5f): a large number of isolated AuNPs but also clusters of metallic structures can be found enclosed in single multivesicular entities close to the nucleus. However, these clusters were all of submicrometer size, i.e., smaller than observed in the MIL images. In Figure 6, the full potential of CARS and MIL microscopy is illustrated by volume images of a HEK cell after 6 h of incubation. The complete movie of the three-dimensional rendering of the cell is available in the Supporting Information section (Movie 1). The three-dimensional distribution of AuNPs in the entire cell volume can be assessed, providing integrated information on density variations throughout the cytoplasm and

dx.doi.org/10.1021/jp2009012 |*J. Phys. Chem. B* XXXX, XXX, 000–000

in the vicinity of important organelles, information difficult to retrieve by TEM. These tomographic CARS/MIL images show the high density of AuNPs evenly distributed throughout the cytoplasm of the keratinocytes.

DISCUSSION

The selectivity of the MIL microscopy toward AuNPs is ascertained by the collection of two spectrally separated signals at 535 nm (bandwidth 25 nm) and 650 nm (bandwidth 50 nm), which show correlated response as expected from the broadband AuNP photoluminescence. In practice, no noteworthy differences were observed in any of the sets of MIL images in the two spectral regions selected for the collection, confirming the negligible contribution from fluorescent biologic components. This is expected, considering that autofluorescence originating from, e.g., flavins, porphyrins, and NAD(P)H is typically detected at wavelengths below 500 nm with a bandwidth of ~50 nm.[49] Thus, in future studies, a single detection channel can be used for the localization of AuNPs using MIL imaging. Measurements of the time decay of the MIL signal further confirm that the detected signal is of photoluminescent origin. In contrast to the nanosecond long lifetimes of autofluorescent, biological components,[50] the signal emitted exhibits significantly faster <200 ps decay as indicated in Figure 2d. This ultrafast emission corresponds well to the characteristics of AuNP photoluminescence previously reported in the literature.[45]

Sensitivity at single-particle level is proven by comparison with TEM measurements (Figures 3 and 5) where AuNPs are mostly found isolated within endosomes separated by more than 300 nm, explained by the plasmonic enhancement of the emitted photoluminescence. Since the resolution of CARS/MIL microscopy is limited to 300 nm, it is impossible to distinguish from the size of the photoluminescence feature a single AuNP from that of a small cluster of AuNPs. Also, due to the broad character of the emission spectrum of AuNPs, the frequency shift of the emission induced by plasmonic coupling is not readily measurable in MIL. Estimation of the number of AuNPs present in a cluster with subresolution dimension is conceivable through intensity calibration of the collected signal, although a simple relationship is not to be expected. Collections of AuNPs cannot be considered as independent scatterers due to the coupling of their plasmons, resulting in collective enhancement effect.[51] Thus, the establishment of a calibration routine requires the support of thorough theoretical analysis, beyond the scope of the present study. A consequence of this collective enhancement is also that large amounts of energy are locally dumped in the immediate vicinity of the AuNPs.[52] Moreover, the probe beams may act as an optical tweezer on large clusters of particles.[53] The particles are then moved while being scanned, which could explain that the AuNP clusters in Figure 5c appear significantly larger than what is observed in the corresponding TEM images. We have indeed observed that the use of lower excitation powers in the laser beams reduces the apparent cluster size in these cells.

One of the surprising results shown in this work is the marked difference in AuNPs uptake between healthy human keratinocytes and a squamous carcinoma cell line. The number of cells investigated prevents a statistical analysis of the uptake process; however, identical behavior was found for all cells investigated for each cellular system, inferring that our results are expected to be of general character. The nonspecific uptake of AuNPs in the two cell lines may be of interest from the perspective of applying functionalized particles for selective drug delivery. Previously, a significantly reduced cellular uptake of AuNPs has been reported after coating the NPs with the neutral ligand PEG, for other cell lines.[21,54,55] The nonreactive surface of the PEG-coated NPs and possible steric hindrance has been suggested to prevent the establishment of active contact with the cell membrane, so that efficient endocytosis cannot take place. While a limited number of isolated AuNPs indeed was found in the SCCs irrespective of incubation time, a significant amount of particles was observed in the keratinocytes by CARS/MIL microscopy. The amount of cellular AuNPs was found to increase with exposure, and the AuNPs were found to be distributed over the entire cell volume. This was independently confirmed by high-resolution TEM of selected cell sections (Figures 2−5). The limited uptake of PEG-coated AuNPs for SCC cells is in accordance with previous observations specifically for SCCs,[32] as well as for other cell lines.[21,54,55] This raises the question why PEG-coated AuNPs are so readily incorporated in epithelial keratinocytes.

Three factors should be taken into account while attempting to explain the different uptake: changes of the surface properties of the AuNPs, difference in the electrostatic properties of the membrane of individual cell lines, and the influence of differences in the composition of the incubation medium on the properties of the cell membrane. The possibility that the surface properties of the PEG-coated AuNPs change upon contact with the different cell culture media, as a result, for instance, of spontaneous functionalization by the adsorption of proteins from the medium,[7,56] is unlikely due to the inert properties of the PEG-coating irrespective of which proteins are present in the medium.[52,57] The possible differences in electrostatic charges of the cell membrane of the two different cell lines is equally unlikely to play a role in the uptake of particles that present neutral charged surface coating. More probable is instead that the different scenarios can be attributed to cell-specific chemical properties. The internalization of AuNPs is a process strongly affected by efficient contact with the cell membrane. The adhesion can be either of nonspecific character, resulting in direct penetration of the NP through the membrane, or mediated by receptors that provide specific adhesion, inducing the formation of NP-carrying endocytic vesicles (for a review on the receptor-mediated internalization pathways see ref 58). With the exception of a few examples,[56,59] details of AuNP internalization are still largely unknown. The presence in high concentrations of human epidermal growth factor (EGF) in the growth medium is known to up-regulate macropinocytosis.[60] In our experiments, EGF was present at low concentration (0.2 ng/mL) in the growth medium employed for the keratinocytes but not for SCCs, and might still contribute to account for increased internalization through this pathway. This hypothesis is supported by the broad size span of the endosomes found in keratinocytes as observed in the TEM images, also including larger sizes (400−800 nm) characteristic for macropinosomes compared to other endosomes.[61] Confirmation of this hypothesis is beyond the aims of this work and can be envisaged in follow-up studies where the concentration of EGF in the medium is varied, although the above observations point toward an issue widely underestimated in studies on particles internalization. While the nano−bio research field spends large efforts on investigating how different properties of the NPs affect the efficiency with which they are incorporated in cells, this study highlights that the incorporation mechanism is as well highly dependent on the cell line used, and perhaps even on the details of the medium.

dx.doi.org/10.1021/jp2009012 |J. Phys. Chem. B XXXX, XXX, 000–000

CONCLUSIONS

Systematic studies on the incorporation mechanisms of AuNPs in living mammalian cells are, at present, limited by the lack of noninvasive imaging techniques. For this purpose, we introduce the combination of CARS and MIL microscopy, offering visual access to the fascinating world where nanomaterials meet living matter thanks to *label-free imaging* of biomolecules and *single-NP sensitivity*. Since no sample preparation is required, a more realistic picture of the three-dimensional distribution of intracellular AuNPs in relation to the components of the cell is provided with high spatial resolution (300 nm lateral and ~2 μm axial), beyond the capabilities of present technology. As an outlook, other cellular components than the lipid-rich cell membrane and subcellular organelles may specifically be targeted in the CARS-channel by probing molecular vibrations characteristic for, e.g., mitochondria and nucleic acids,[62,63] opening up for colocalization of AuNPs with further organelles without labeling.

The observations reported in the current work have implications both for (i) fundamental studies of NP-uptake mechanism and (ii) for clinical applications of NPs. Our work highlights the need for detailed characterization of the incorporation mechanisms used by *different* cell models, as they appear to be cell specific probably as a result of the individual composition of the cell membrane; in contrast to squamous carcinoma cells and precious studies on several other cell lines, PEG-coated AuNPs are readily incorporated in healthy human epithelial keratinocytes. Thus, it is difficult to draw any general conclusions from fundamental studies of uptake mechanisms involving a single-cell model and it raises the need for detailed characterization of the composition of the cell membrane. The clinical consequence of this observation is that PEG coating may not be sufficient to prevent an undesirable, general uptake of NPs in conjunction with transdermal delivery of NP-based therapeutic and diagnostic agents. This adds to the need for more sophisticated coatings in order to avoid the potentially toxic accumulation of NPs in healthy cells, toward safe and efficient transdermal delivery of drugs, gene-regulating therapeutics and diagnostic agents only targeting diseased cells. As a promising alternative, nanoparticles labeled with anti-epidermal growth factor receptor (anti-EGFR) have been recently demonstrated to selectively target tumor cells through specific binding.[64] With the ability of 3-dimensional imaging of the distribution of functionalized AuNPs in living cells at single-particle sensitivity and without the need for labeling or sectioning, our work illustrates that CARS/MIL microscopy has the potential to become an important instrument for the development of further functional coatings as well as within the nano-bio research field in general.

ASSOCIATED CONTENT

Supporting Information. Movie 1, three-dimensional rendering of a HEK cell after 6 h of incubation with AuNPs. This material is available free of charge via the Internet at http://pubs.acs.org.

AUTHOR INFORMATION

Corresponding Author
*E-mail: enejder@chalmers.se.

ACKNOWLEDGMENT

The authors thank Dr. K. F. Domke, Dr. R. K. Campen, and Dr. J. P. R. Day for discussions and Dr. C. Brackmann for technical support.

This study was financially supported by the Swedish Research Council (B.B., F.S., M.E., A.E.), the Göteborg Science Centre for Molecular Skin Research at University of Gothenburg (M.E., B.B.), the Nederlandse Organisatie voor Wetenschappelijk Onderzoek (Netherlands Organization for the Advancement of Research) (M.B., G.R.), and the COST Action MP0603 microCARS (G.R.).

REFERENCES

(1) Ghosh, P.; Han, G.; De, M.; Kim, C. K.; Rotello, V. M. *Adv. Drug Delivery Rev.* **2008**, *60*, 1307.
(2) Jain, P. K.; Huang, X. H.; El-Sayed, I. H.; El-Sayed, M. A. *Acc. Chem. Res.* **2008**, *41*, 1578.
(3) Eustis, S.; El-Sayed, M. A. *Chem. Soc. Rev.* **2006**, *35*, 209.
(4) Connor, E. E.; Mwamuka, J.; Gole, A.; Murphy, C. J.; Wyatt, M. D. *Small* **2005**, *1*, 325.
(5) Cui, H. F.; Vashist, S. K.; Al-Rubeaan, K.; Luong, J. H. T.; Sheu, F. S. *Chem. Res. Toxicol.* **2010**, *23*, 1131.
(6) Hardman, R. *Environ. Health Perspect.* **2006**, *114*, 165.
(7) Chithrani, B. D.; Ghazani, A. A.; Chan, W. C. W. *Nano Lett.* **2006**, *6*, 662.
(8) Kumar, S.; Aaron, J.; Sokolov, K. *Nature Protocols* **2008**, *3*, 314.
(9) Levy, R.; Thanh, N. T. K.; Doty, R. C.; Hussain, I.; Nichols, R. J.; Schiffrin, D. J.; Brust, M.; Fernig, D. G. *J. Am. Chem. Soc.* **2004**, *126*, 10076.
(10) Mandal, D.; Maran, A.; Yaszemski, M. J.; Bolander, M. E.; Sarkar, G. *J. Mater. Sci.: Mater. Med.* **2009**, *20*, 347.
(11) Pujals, S.; Bastus, N. G.; Pereiro, E.; Lopez-Iglesias, C.; Punte, V. F.; Kogan, M. J.; Giralt, E. *Chembiochem* **2009**, *10*, 1025.
(12) Giljohann, D. A.; Seferos, D. S.; Patel, P. C.; Millstone, J. E.; Rosi, N. L.; Mirkin, C. A. *Nano Lett.* **2007**, *7*, 3818.
(13) Patel, P. C.; Giljohann, D. A.; Seferos, D. S.; Mirkin, C. A. *Proc. Natl. Acad. Sci. U.S.A.* **2008**, *105*, 17222.
(14) Sepulveda, B.; Angelome, P. C.; Lechuga, L. M.; Liz-Marzan, L. M. *Nano Today* **2009**, *4*, 244.
(15) Verma, A.; Stellacci, F. *Small* **2010**, *6*, 12.
(16) Chithrani, D. B.; Dunne, M.; Stewart, J.; Allen, C.; Jaffray, D. A. *Nanomed.: Nanotechnol. Biol. Med.* **2010**, *6*, 161.
(17) Ghosh, P.; Yang, X. C.; Arvizo, R.; Zhu, Z. J.; Agasti, S. S.; Mo, Z. H.; Rotello, V. M. *J. Am. Chem. Soc.* **2010**, *132*, 2642.
(18) Giljohann, D. A.; Seferos, D. S.; Daniel, W. L.; Massich, M. D.; Patel, P. C.; Mirkin, C. A. *Angew. Chem., Int. Ed.* **2010**, *49*, 3280.
(19) Dixit, V.; Van den Bossche, J.; Sherman, D. M.; Thompson, D. H.; Andres, R. P. *Bioconjugate Chem.* **2006**, *17*, 603.
(20) El-Sayed, I. H.; Huang, X. H.; El-Sayed, M. A. *Cancer Lett.* **2006**, *239*, 129.
(21) Eghtedari, M.; Liopo, A. V.; Copland, J. A.; Oraevslty, A. A.; Motamedi, M. *Nano Lett.* **2009**, *9*, 287.
(22) Paciotti, G. F.; Myer, L.; Weinreich, D.; Goia, D.; Pavel, N.; McLaughlin, R. E.; Tamarkin, L. *Drug Delivery* **2004**, *11*, 169.
(23) Chen, Y. H.; Tsai, C. Y.; Huang, P. Y.; Chang, M. Y.; Cheng, P. C.; Chou, C. H.; Chen, D. H.; Wang, C. R.; Shiau, A. L.; Wu, C. L. *Mol. Pharm.* **2007**, *4*, 713.
(24) Gibson, J. D.; Khanal, B. P.; Zubarev, E. R. *J. Am. Chem. Soc.* **2007**, *129*, 11653.
(25) Patra, C. R.; Bhattacharya, R.; Wang, E. F.; Katarya, A.; Lau, J. S.; Dutta, S.; Muders, M.; Wang, S. F.; Buhrow, S. A.; Safgren, S. L.; Yaszemski, M. J.; Reid, J. M.; Ames, M. M.; Mukherjee, P.; Mukhopadhyay, D. *Cancer Res.* **2008**, *68*, 1970.
(26) Agasti, S. S.; Chompoosor, A.; You, C. C.; Ghosh, P.; Kim, C. K.; Rotello, V. M. *J. Am. Chem. Soc.* **2009**, *131*, 5728.
(27) Aryal, S.; Grailer, J. J.; Pilla, S.; Steeber, D. A.; Gong, S. Q. *J. Mater. Chem.* **2009**, *19*, 7879.
(28) Brown, S. D.; Nativo, P.; Smith, J. A.; Stirling, D.; Edwards, P. R.; Venugopal, B.; Flint, D. J.; Plumb, J. A.; Graham, D.; Wheate, N. J. *J. Am. Chem. Soc.* **2010**, *132*, 4678.

(29) Schrand, A. M.; Schlager, J. J.; Dai, L. M.; Hussain, S. M. *Nature Protocols* **2010**, *5*, 744.
(30) Shukla, R.; Bansal, V.; Chaudhary, M.; Basu, A.; Bhonde, R. R.; Sastry, M. *Langmuir* **2005**, *21*, 10644.
(31) Qian, X. M.; Peng, X. H.; Ansari, D. O.; Yin-Goen, Q.; Chen, G. Z.; Shin, D. M.; Yang, L.; Young, A. N.; Wang, M. D.; Nie, S. M. *Nat. Biotechnol.* **2008**, *26*, 83.
(32) Curry, A. C.; Crow, M.; Wax, A. *J. Biomed. Opt.* **2008**, 13.
(33) Wax, A.; Sokolov, K. *Laser Photonics Rev.* **2009**, *3*, 146.
(34) Wilcoxon, J. P.; Martin, J. E.; Parsapour, F.; Wiedenman, B.; Kelley, D. F. *J. Chem. Phys.* **1998**, *108*, 9137.
(35) Beversluis, M. R.; Bouhelier, A.; Novotny, L. *Phys. Rev. B* **2003**, *68*, 115433.
(36) Farrer, R. A.; Butterfield, F. L.; Chen, V. W.; Fourkas, J. T. *Nano Lett.* **2005**, *5*, 1139.
(37) Durr, N. J.; Larson, T.; Smith, D. K.; Korgel, B. A.; Sokolov, K.; Ben-Yakar, A. *Nano Lett.* **2007**, *7*, 941.
(38) Dowling, M. B.; Li, L. J.; Park, J.; Kumi, G.; Nan, A.; Ghandehari, H.; Fourkas, J. T.; DeShong, P. *Bioconjugate Chem.* **2010**, *21*, 1968.
(39) Fujita, K.; Smith, N. I. *Mol. Cells* **2008**, *26*, 530.
(40) Enejder, A.; Brackmann, C.; Svedberg, F. *Sel. Top. Quantum Electron., IEEE J.* **2010**, *16*, 506.
(41) Cheng, J. X.; Jia, Y. K.; Zheng, G. F.; Xie, X. S. *Biophys. J.* **2002**, *83*, 502.
(42) Evans, C. L.; Potma, E. O.; Puoris'haag, M.; Cote, D.; Lin, C. P.; Xie, X. S. *Proc. Natl. Acad. Sci. U.S.A.* **2005**, *102*, 16807.
(43) Hellerer, T.; Axang, C.; Brackmann, C.; Hillertz, P.; Pilon, M.; Enejder, A. *Proc. Natl. Acad. Sci. U.S.A.* **2007**, *104*, 14658.
(44) Kempa, T.; Farrer, R. A.; Giersig, M.; Fourkas, J. T. *Plasmonics* **2006**, *1*, 45.
(45) Varnavski, O. P.; Mohamed, M. B.; El-Sayed, M. A.; Goodson, T. *J. Phys. Chem. B* **2003**, *107*, 3101.
(46) Zhang, Y.; Yu, J.; Birch, D. J. S.; Chen, Y. *J. Biomed. Opt.* **2010**, *15*, 020504.
(47) Cheng, J. X.; Volkmer, A.; Xie, X. S. *J. Opt. Soc. Am. B* **2002**, *19*, 1363.
(48) Alberts, B., Bray, D., Lewis, J., Raff, M., Roberts, K., Watson, J. D. *Molecular Biology of the Cell*; Garland Publishing Inc.: New York, 1994.
(49) Billinton, N.; Knight, A. W. *Anal. Biochem.* **2001**, *291*, 175.
(50) Valeur, B. *Molecular Fluorescence: Principles and Applications*; Wiley-VCH: Weinheim, Germany, 2001.
(51) Ghosh, S. K.; Pal, T. *Chem. Rev.* **2007**, *107*, 4797.
(52) Ehrenberg, M. S.; Friedman, A. E.; Finkelstein, J. N.; Oberdorster, G.; McGrath, J. L. *Biomaterials* **2009**, *30*, 603.
(53) Hajizadeh, F.; Reihani, S. N. *Opt. Express* **2010**, *18*, 551.
(54) Liu, C. J.; Wang, C. H.; Chien, C. C.; Yang, T. Y.; Chen, S. T.; Leng, W. H.; Lee, C. F.; Lee, K. H.; Hwu, Y.; Lee, Y. C.; Cheng, C. L.; Yang, C. S.; Chen, Y. J.; Je, J. H.; Margaritondo, G. *Nanotechnology* **2008**, *19*, 295104.
(55) Nativo, P.; Prior, I. A.; Brust, M. *ACS Nano* **2008**, *2*, 1639.
(56) Chithrani, B. D.; Chan, W. C. W. *Nano Lett.* **2007**, *7*, 1542.
(57) Wuelfing, W. P.; Gross, S. M.; Miles, D. T.; Murray, R. W. *J. Am. Chem. Soc.* **1998**, *120*, 12696.
(58) Conner, S. D.; Schmid, S. L. *Nature* **2003**, *422*, 37.
(59) Brandenberger, C.; Muhlfeld, C.; Ali, Z.; Lenz, A. G.; Schmid, O.; Parak, W. J.; Gehr, P.; Rothen-Rutishauser, B. *Small* **2010**, *6*, 1669.
(60) Haigler, H. T.; McKanna, J. A.; Cohen, S. *J. Cell Biol.* **1979**, *83*, 82.
(61) Swanson, J. A.; Watts, C. *Trends Cell Biol* **1995**, *5*, 424.
(62) Pully, V. V.; Otto, C. *J. Raman Spectrosc.* **2009**, *40*, 473.
(63) Chiu, L.; Ando, M.; Hamaguchi, H. *J. Raman Spectrosc.* **2010**, *41*, 2.
(64) Crow, M. J.; Grant, G.; Provenzale, J. M.; Wax, A. *Am. J. Roentgenol.* **2009**, *192*, 1021.